Intra-grain local luminescence properties of $CdSe_{0.1}Te_{0.9}$ Thin Films

Ganga R. Neupane[1,2], David S. Albin[3], Joel N. Duenow[3], Matthew O. Reese[3], Susanna Thon[2], and Behrang H. Hamadani[1]

[1]National Institute of Standards & Technology, Gaithersburg, MD 20899, USA
[2]Johns Hopkins University, Baltimore, MD 21218, USA
[3]National Renewable Energy Laboratory, Golden, CO 80401, USA

We report on the local photoluminescence properties of grains and grain boundaries of $CdSe_{0.1}Te_{0.9}$ thin film deposited by the colossal grain growth method using a wide-field hyperspectral imaging technique. We observed significant variations in the photoluminescence intensity of both individual grains and also that of grain boundaries. Multiple sub-bandgap defect peaks were captured in the luminescence spectra in the energy range 1.2 eV to 1.6 eV. The intensity and peak positions of these sub-gap emissions were slightly different among various grains and at the grain boundaries, revealing intra- and inter-grain variations in these polycrystalline thin films. A recently-developed density-of-states based photoluminescence model was extended to include multiple peaks and was fitted to the data. We observed that at a fixed temperature, the quasi-Fermi level splitting energy and a disordered energy parameter can be extracted locally by this model.

I. Introduction

Wide-field, luminescence-based hyperspectral (HS) imaging is a unique and powerful technique that can acquire high resolution images over many continuous spectral bands [1]. Every pixel in the hyperspectral image contains the full spectral information, therefore, making it a useful tool for assessing local charge transport properties of thin-film photovoltaic materials.

The performance of thin-film cadmium telluride (CdTe) solar cells have continued to improve in recent years, owing to refinements in passivation techniques such as alloying of CdTe with Se, select doping and $CdCl_2$ treatment, to reduce defect-mediated non-radiative recombination [2], [3]. However, high resolution luminesence imaging that can visualize local recombination phenomena and the role of defects at the grain interiors (GIs) and grain boundaries (GBs) has not been performed extensively. Wide field HS imaging is an attractive technique to quickly and reliably image large areas of the film and investigate local potential fluctuations or variations in defect-related emissions between the grains.

Small-grain polycrystalline CdTe films have poor electro-optical properties. The local charge transport in CdTe is significantly impacted by the size of the grains and the defects associated with them. In addition, it has been found that the carrier lifetime, which correlates well with the open circuit voltage, V_{oc}, increases with grain size [2]. So we need to focus on increasing the size of CdTe thin film grains and passivating the local defects and interfaces. In this work, we have used the colossal grain growth (CGG) [4] method to produce large-grain CdSeTe thin films so that they can be used as a template for the epitaxial growth of large-grained CdTe thin films. Studying the absolute photoluminescence (PL) images obtained from these films, we find that there are both intra-grain and inter-grain variations in the luminsence spectra at the micron scale. To understand how these variations lead to local differences in the chemical potential or the disordered energy, we have used and extended a recent single-transition analytical PL model [5] to a multi-transition regime such as seen in data presented in the results. We show that it is possible to model a complicated multi-peak PL emission spectrum using a single quasi-Fermi level splitting (QFLS) energy and extract the sub-gap absorptivity and the disordered energy of the various sub-gap peaks by use of this model. Explaining local variability through useful quantities such as the QFLS energy can improve materials growth.

II. Methods

A. Sample preparation

The polycrystalline thin film of CdSeTe was formed on alumina-coated glass substrates. The film was made using a different growth technique called the CGG method. A 3.0 μm CdSeTe precursor film was evaporated onto a 0.7 mm thick alumino-borosilicate glass substrate coated with 100 nm of alumina heated to about 400 °C. Evaporation was from a single-source alumina crucible containing an alloy of $CdSe_{0.1}Te_{0.9}$ heated to 660 °C to produce a deposition flux close to 10 A/s. In the subsequent CGG step, the CdSeTe precursor film is then heated to 550 °C while suspended 1 mm, film-side down, above a Se-containing powder (typically, $CdSe_{0.4}Te_{0.6}$) in an atmosphere of 100-Torr helium (13332.2 Pascal). After the CGG step, the CdSeTe film was then annealed and suspended over a powder of $CdCl_2$ at 550 °C for 10 min in an ambient of 400-Torr helium (53328.9 Pascal) to reduce recombination and increase luminescence efficiency. Details about the CGG process can be found in [4].

B. Hyperspectral characterization

HS imaging in PL mode was performed in the spectral region from 780 nm to 980 nm using a silicon-based CCD camera system with an appropriate HS grating. A 20X

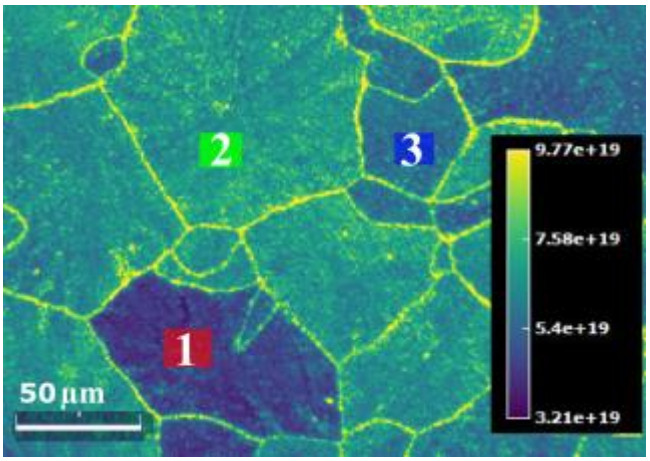

Fig. 1. A PL image of grains and grain boundaries of CdSeTe thin film at 144 K at a fixed intensity of 1776 W/m^2. The colorbar shows the absolute photon flux in units of photons/m^2 s eV.

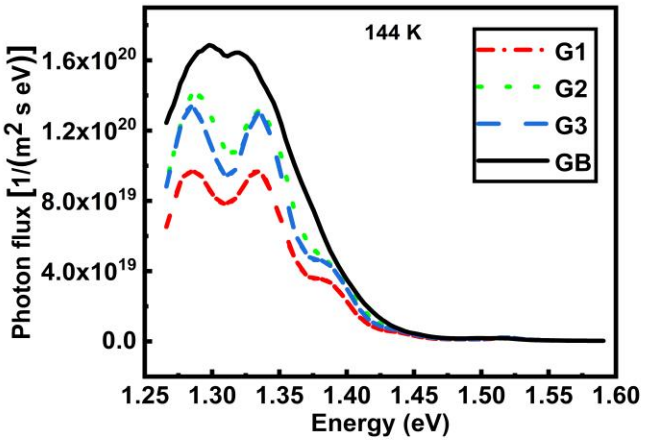

Fig. 2. PL spectra for select grains and a grain boundary at 144 K.

microscope objective was used for capturing the images shown here. For the PL excitation, a 532 nm laser was used to illuminate the entire field of view. Temperature-dependent measurements were performed using a liquid nitrogen flow optical cryostat under vacuum.

III. Results

Fig. 1 shows the PL photon flux emission map of a $CdCl_2$ treated CdSeTe thin film at 144 K (temperature estimated from the energetic position of the band-to-band peak) taken at 1.36 eV. These measurements have been performed at lower temperatures because the radiative efficiency is too low near room temperature to provide the level of detail and clarity observed here. Surprisingly, the image reveals a higher luminescence intensity at the location of the GBs. This suggests less non-radiative recombination at GBs compared to the GIs. The treatment of as-grown films by $CdCl_2$ results in overall passivation of both GIs and GBs, but the passivation is stronger at the GBs. Other studies have also reported GB defect passivation using Se and $CdCl_2$ treatments [6], [7]. In addition, the image also shows a variety of grains with different sizes. The grains are tens of µm in lateral dimension and from the image, it is clear that these grains do not have a uniform defect profile, revealing a remarkable carrier recombination non-uniformity.

Next, we select three grain interiors and one grain boundary to study their spectral emission profile as shown in Fig. 1 labelled as 1, 2 and 3 for the respective grains. These grains are chosen in a such a way that they look different in terms of their size and PL brightness. The PL spectra corresponding to several GIs and one GB are shown in Fig 2. The spectra consist of several peaks in the range of ~ 1.2 eV to 1.6 eV. The intensity and peak position energies corresponding to each grain are a little different. This is either due to variations in the individual grain structures or variability in the defect distribution across the various grains. Since the band-to-band (BB) transition is around 1.52 eV, all these sub-bandgap transitions are related to radiative defects with energies smaller than E_g. These transitions likely stem from donor-acceptor pair defects in this material but further investigation is needed to confirm their characteristics. In addition, the observed multiple PL peaks blend together at the GB sites and form a large broadened peak. This blending of the peaks at the GB sites is due to inherent disorder/ other factors at the boundary. Because the crystalline nature of the material is disrupted at the GB, this energetic broadening is expected. Interestingly, the intensity of the PL emission at the GB is higher across all emitting energies than the grain interiors. Also, we observe (not shown here) that the BB energy is slightly lower at the GBs than GIs, suggesting a slightly higher aggregation of Se at the GBs, which may help with better passivation of GB defects.

To understand the nature of the PL emission spectra better, we extend a single-transition model developed by Katahara and Hillhouse [5] to include multiple optical transitions. Since absolute photon flux spectra are measured in our HS system, this model can be used to estimate important physical parameters such as the quasi-Fermi level splitting energy, Δµ, the sub-gap absorption coefficient α and the energy broadening paramenter γ (i.e., Urbach energy). The spontaneous radiative emission in terms of the spectral absorptivity under non-equilibrium condition is given by [5], [8]:

$$I_{PL}(E) = \frac{2\pi}{h^3c^2}\frac{E^2 a(E)}{\exp\left(\frac{E-\Delta\mu}{kT}\right)-1} \quad (1)$$

where I_{PL} is the photoluminescence intensity, h is the Planck constant, a is the absorptivity, k is the Boltzmann constant, and T is the temperature. The absorptivity is defined in terms of a joint density of states $G_i(E)$ for each emission peak that includes a disordered sub-bandgap tail parameter γ_i, $a(E) \sim \sum \alpha_{0i} G_i(E)$, where α_{0i} is absorption coefficient in the high energy side of the

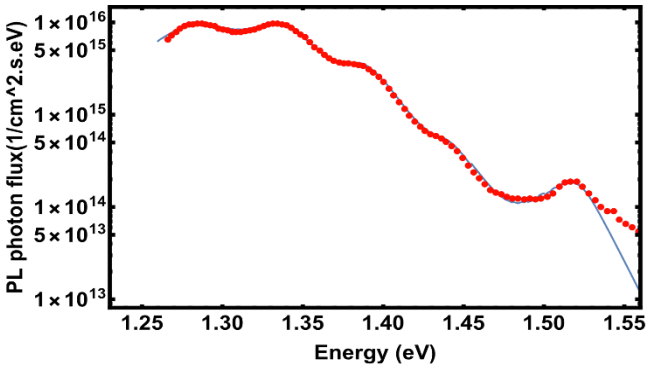

Fig. 3. Log-linear plot of PL spectra of G1 with the multi-peak modeling

peak. Figures 3 and 4 demonstrate how this model, summed over multiple transitions, can be used to fit our data. For the simplicity, we choose to show the fitting for G1 and the GB. In the figure, the red symbols are the experimental PL spectra and the solid blue lines are the model-calculated spectra. For a fixed *T*, the intensity of the PL emission is controlled by both the $\Delta\mu$ and the absorption coefficients α_{0i}. We find that we can fix α_{01} of the BB peak (peak on the furthest right) to a reasonable value of ~ 10^4 cm^{-3} and then focus on determing a single $\Delta\mu$ parameter along with α_{0i} for all the below-gap peaks. The disordered energy parameters γ_i can be changed to increase or decrease the low-energy tail broadening of each peak such that the composite curve fits the data. $\Delta\mu$ values for G1, G2, and G3 are 1.265 eV, 1.267 eV, and 1.266 eV respectively and 1.269 eV for the GB. This supports the notion that a higher non-radiative recombination leads to a lower quasi-Fermi level splitting energy or a lower internal voltage. Similarly, we found that the grain boundary is more disordered ($\gamma = 12.5$ meV) than the grain interior ($\gamma = 10.3$ meV) near the band edge

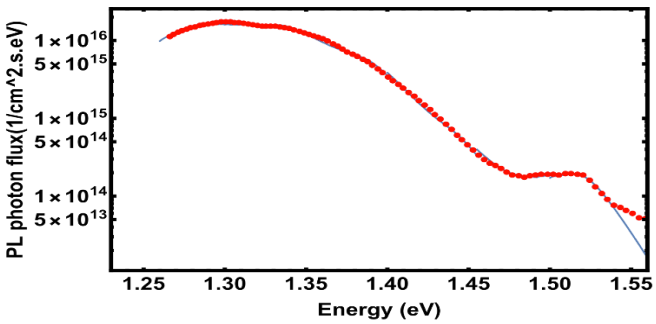

energy. This explains our observation of broadening of the low energy PL tail of the grain boundary.

Fig. 4. Log-linear plot of PL spectra of GB with the model fitting.

IV. Summary

We have presented high resolution PL images of CdSeTe thin films using a wide-field hyperspectral imaging system. Higher defect passivation at the GBs results in a higher luminescence signal there compared to grain interiors. Different sizes of grains and brightness differences reveal remarkable grain-to-grain and grain-to-grain boundary variations which strongly depend on the defect distribution. In addition, a density of states-based model was successfully extended to fit multiple peaks in the PL spectra and different parameters like the quasi-Fermi level splitting energy and the sub-bandgap disorder energy were extracted from each individual peak. The disorder energy at the grain boundaries is higher than grain interiors, causing several defect transitions to blend together.

References

[1] B. H. Hamadani, M. A. Stevens, B. Conrad, M. P. Lumb, and K. J. Schmieder, "Visualizing localized, radiative defects in GaAs solar cells," *Sci Rep*, vol. 12, no. 1, p. 14838, Sep. 2022, doi: 10.1038/s41598-022-19187-4.

[2] H. Nazem, H. P. Dizaj, and N. E. Gorji, "Modeling of J sc and V oc versus the grain size in CdTe, CZTS and Perovskite thin film solar cells," *Superlattices Microstruct*, vol. 128, no. February, pp. 421–427, 2019, doi: 10.1016/j.spmi.2019.02.002.

[3] R. M. Geisthardt, M. Topič, and J. R. Sites, "Status and Potential of CdTe Solar-Cell Efficiency," *IEEE J Photovolt*, vol. 5, no. 4, pp. 1217–1221, Jul. 2015, doi: 10.1109/JPHOTOV.2015.2434594.

[4] D. S. Albin, M. Amarasinghe, M. O. Reese, J. Moseley, H. Moutinho, and W. K. Metzger, "Colossal grain growth in Cd(Se,Te) thin films and their subsequent use in CdTe epitaxy by close-spaced sublimation," *Journal of Physics: Energy*, vol. 3, no. 2, p. 024003, Apr. 2021, doi: 10.1088/2515-7655/abd297.

[5] J. K. Katahara and H. W. Hillhouse, "Quasi-Fermi level splitting and sub-bandgap absorptivity from semiconductor photoluminescence," *J Appl Phys*, vol. 116, no. 17, p. 173504, Nov. 2014, doi: 10.1063/1.4898346.

[6] N. A. Shah, A. Ali, S. Hussain, and A. Maqsood, "CdCl2-treated CdTe thin films deposited by the close spaced sublimation technique," *J Coat Technol Res*, vol. 7, no. 1, pp. 105–110, 2010, doi: 10.1007/s11998-008-9146-0.

[7] R. Wang, M. Lan, and S.-H. Wei, "Enhanced performance of Se-alloyed CdTe solar cells: The role of Se-segregation on the grain boundaries," *J Appl Phys*, vol. 129, no. 2, p. 024501, Jan. 2021, doi: 10.1063/5.0036701.

[8] M. Tebyetekerwa *et al.*, "Quantifying Quasi-Fermi Level Splitting and Mapping its Heterogeneity in Atomically Thin Transition Metal Dichalcogenides," *Advanced Materials*, vol. 31, no. 25, pp. 1–8, 2019, doi: 10.1002/adma.201900522.